

A CGC/saturation approach for angular correlations in proton-proton scattering.

E. Gotsman^{a*}, E. Levin^{a,b†} and I. Potashnikova^{b‡}

a) Department of Particle Physics, School of Physics and Astronomy, Raymond and Beverly Sackler Faculty of Exact Science, Tel Aviv University, Tel Aviv, 69978, Israel

b) Departamento de Física, Universidad Técnica Federico Santa María, Avda. España 1680 and Centro Científico-Tecnológico de Valparaíso, Casilla 110-V, Valparaíso, Chile

ABSTRACT: We generalized our model for the description of hard processes, and calculate the value of the azimuthal angle correlations (Fourier harmonics v_n), for proton-proton scattering. The energy and multiplicity independence, as well as the value of v_n , turn out to be in accord with the experimental data, or slightly larger. Therefore, before making extreme assumptions on proton-proton collisions, such as the production of quark-gluon plasma in the large multiplicity events, we need to explain how these effect the Bose-Einstein correlations which are so large, that have to be taken into account, and which are able to describe the angular correlations in proton-proton collisions, without including final state interactions.

KEYWORDS: Soft Pomeron, BFKL Pomeron, Diffractive Cross Sections, Rapidity Correlations, Hard processes, Azimuthal angle Correlations.

PACS: 13.85.-t, 13.85.Hd, 11.55.-m, 11.55.Bq

*Email: gotsman@post.tau.ac.il.

†Email: leving@post.tau.ac.il

‡Email: irina.potashnikova@usm.cl

Contents

1. Introduction	2
2. The model	3
2.1 Theoretical input from the CGC/saturation approach	3
2.2 Phenomenology: assumptions and new small parameters	5
2.3 Results of the fit	8
3. Deep inelastic scattering	8
3.1 Generalities	8
3.2 Modification to also include DIS	10
3.3 The description of the HERA data	11
4. Inclusive production	11
5. Azimuthal angle correlations	13
5.1 Double inclusive cross section	13
5.2 Bose-Einstein correlation: energy dependence	15
5.3 Bose-Einstein correlation: values of v_n and its multiplicity dependence	16
5.4 Bose-Einstein correlation: contribution of the semi-enhanced and enhanced diagrams (diffraction production of large masses)	18
5.5 Comparison with the experiment	20
6. Conclusions	21

1. Introduction

The experimental data on azimuthal angle correlations (see Refs. [1–11] show suprising similarities between different processes: nucleus-nucleus, hadron-nucleus and hadron-hadron collisions. The popular explanation is related to elliptic flow, and stems from the interaction in the final state. In the framework of such an approach, we have to assume that the proton interactions are similar to nucleus scattering, at least for events with large multiplicity. However, the ATLAS data [9] show that $v_{2,2}, v_{3,3}$ and $v_{4,4}$ do not depend on multiplicity at $W=13$ TeV and at $W= 2.76$ TeV.

In this paper we will discuss these correlations from a different point of view. We believe that the general origin of the azimuthal angle correlations in all reactions, stems from the Bose-Einstein correlations (BEC) of the produced gluons, which originate from the gluon wave function in the initial state [12–21]. The attractive feature of this idea is that, BEC have a general source that characterizes the volume of the interaction [22,23]. Therefore, the main dimensional parameters of the interaction that manifest themselves in diffraction scattering, and in inclusive production, should determine the BEC. In other words, that in spite of the embryonic stage of our understanding of the confinement of quarks and gluons, we can develop a quantitative approach for the BEC in the framework of a model for soft interactions at high energy. To accomplish this, we need to construct such a model, that will allow us to discuss soft and hard processes on the same footing.

The main goal of this paper is to develop such model. Fortunately, we have built a model which provides a good description of all the soft data [24–29], including, total, inelastic, elastic and diffractive cross sections, the t -dependence of these cross sections as well as the inclusive production and rapidity correlations. In this paper we expand this model to include the hard interactions mostly using the geometric scaling behavior of the scattering amplitude [30] for the hard kinematic region in the Colour Glass Condensate (CGC)/saturation approach [31].

The idea of BEC being the main source of the azimuthal angle correlations, is marred by the observation [15,16], that the process of the central diffraction production of colourless gluon dijets, gives a contribution which is equal to that of the BEC. In this case $v_{n,n}$ with odd n are equal to zero, while $v_{n,n}$ with even n , are twice larger. We will not discuss this problem here. Our main goal is to obtain reliable quantitative estimates for $v_{n,n}$. However, we believe that due to the Sudakov suppression in Double Log Approximation of perturbative QCD, the dijet contribution is negligibly small [32].

The paper is organized as follows. In the next section we give a brief review of our model which is based on CGC/saturation approach. We discuss what we have taken from the theory in our approach, and what we have considered from a pure phenomenological approach. We will attempt to clarify the physical meaning of the introduced phenomenological parameters, and show how we include three dimensional sizes, which have been used to describe the scattering amplitude. In the language of the Constituent Quark Model these three sizes are the hadron radius, the size of the constituent quark, and the saturation momentum, which is a typical scale for the high energy amplitude.

In section 3 we generalize our model including the construction of an amplitude at short distances, which is able to describe the deep inelastic scattering (DIS). We compare our amplitude with HERA

experimental data [33]. In section four we calculate the inclusive cross section, and show that we obtain good agreement with the experimental data. This is very important for our calculation, since it demonstrates that we are able to describe the experimental data for inclusive production not only at short distances, but also at long distances.

In section 5 we calculate the value of BEC correlations, its energy and multiplicity dependence. We obtain the value of v_n which are a bit larger than the experimental ones, with a mild dependence on energy and multiplicity. We consider these estimates as the first quantitative prediction for v_n in proton-proton scattering, which are in agreement with the values of the inclusive cross sections, and the cross sections for the hard processes.

In section 6 we draw our conclusions and outline the problems for future investigations.

2. The model

2.1 Theoretical input from the CGC/saturation approach

In this section we generalize our model for soft interactions at high energy [24–29] to include a description of hard processes. This model incorporates two ingredients: the achievements of the CGC/saturation approach, which is an effective theory for QCD at high energy; and the pure phenomenological treatment of the long distance non-perturbative physics, due to the lack of the theoretical understanding of confinement of quark and gluons.

We wish to stress that the most of this section does not contain new results, it reviews our approach, and it is included in the paper only for the sake of completeness of presentation. One can find more details in Refs. [24–29].

The effective theory for QCD at high energies exists in two different formulations: the CGC/saturation approach [34–37], and the BFKL Pomeron calculus [38–51]. In building our model we rely on the BFKL Pomeron calculus, as the relation to diffractive physics and soft processes in general, is more transparent in this approach. However, we believe the CGC/saturation approach produces a more general pattern [49, 50] for the treatment of high energy QCD. Fortunately, in Ref. [50] it was shown, that these two approaches are equivalent for

$$Y \leq \frac{2}{\Delta_{\text{BFKL}}} \ln \left(\frac{1}{\Delta_{\text{BFKL}}^2} \right) \quad (2.1)$$

where Δ_{BFKL} denotes the intercept of the BFKL Pomeron. As we will see, in our model $\Delta_{\text{BFKL}} \approx 0.2 - 0.25$ leading to $Y_{\text{max}} = 20 - 30$, which covers all accessible energies.

The main ingredient, that we need to find, is the resulting (dressed) BFKL Pomeron Green function, which can be calculated using t -channel unitarity constraints:

$$G_{\mathbb{P}}^{\text{dressed}}(Y, r, R; b) = \int \prod_{i=1} d^2 r_i d^2 b_i d^2 r'_i d^2 b'_i N(Y - Y', r, \{r_i, b - b_i\}) \boxed{A_{\text{dipole-dipole}}^{\text{BA}}(r_i, r'_i, \vec{b}_i - \vec{b}'_i)} N(Y', R, \{r'_i, b'_i\}) \quad (2.2)$$

where $N(Y - Y', r, \{r_i, b - b_i\})$ denotes the amplitude for the production in the t -channel of the set of dipoles with $Y = Y'$ and with the size r_i , at the impact parameters b_i . $A_{\text{dipole-dipole}}^{BA}$ denotes the dipole-dipole scattering amplitude in the Born approximation of perturbative QCD, which are indicated by red circles in Fig. 1-a. In addition, in Ref. [50] it is shown that for such Y , we can safely use the Mueller-Patel-Salam-Iancu (MPSI) approach [52]. In this approximation we estimate the amplitudes N in Eq. (2.2), using BFKL Pomeron 'fan' diagrams (see Fig. 1-a for examples of such diagrams). In other words, we can use the parton cascade of the Balitsky-Kovchegov [36] equation, to find the amplitude for the production of dipoles of size r_i at impact parameters b_i . This amplitude can be written as (see Fig. 1-c)

$$\begin{aligned} N(Y - Y', r, \{r_i, b_i\}) &= N^{\text{BK}}(Y - Y', r, \{r_i, b_i\}) \\ &= \sum_{n=1}^{\infty} (-1)^{n+1} \tilde{C}_n(r) \prod_{i=1}^n G_{\mathbb{P}}(Y - Y'; r, r_i, b_i) = \sum_{n=1}^{\infty} (-1)^{n+1} \tilde{C}_n(r) \prod_{i=1}^n G_{\mathbb{P}}(z - z_i). \end{aligned} \quad (2.3)$$

$G_{\mathbb{P}}$ denotes the Green function of the BFKL Pomeron. In the last equation we used the fact that in the saturation region this Green function has geometric scaling behavior, and so it depends on one variable: $z_i = \ln(Q_s^2(Y')r_i^2)$, where $Q_s(Y')$, is the saturation scale, in the vicinity of the saturation scale [53]

$$G_{\mathbb{P}}(z_i) = \phi_0 (r_i^2 Q_s^2(Y, b_i))^{1-\gamma_{cr}} \quad (2.4)$$

where $\gamma_{cr} = 0.37$.

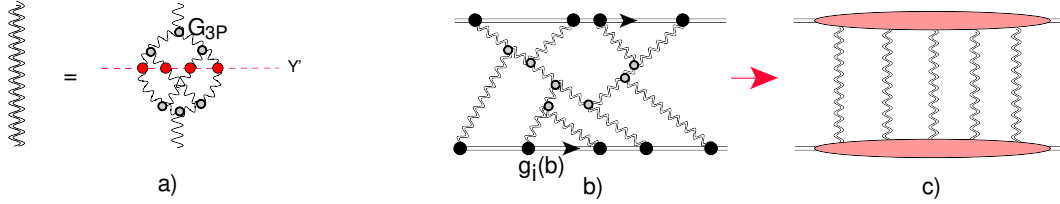


Figure 1: Fig. 1-a shows the set of diagrams in the BFKL Pomeron calculus that produce the resulting (dressed) Green function of the Pomeron in the framework of high energy QCD. The red blobs denote the amplitude for the dipole-dipole interaction at low energy. In Fig. 1-b the net diagrams, which include the interaction of the BFKL Pomerons with colliding hadrons, are shown. The sum of the diagrams after integration over positions of $G_{3\mathbb{P}}$ in rapidity, reduces to Fig. 1-c.

In Ref. [51], it was shown that, the solution to the non-linear BK equation has the following general form

$$N(G_{\mathbb{P}}(\phi_0, z)) = \sum_{n=1}^{\infty} (-1)^{n+1} C_n(\phi_0) G_{\mathbb{P}}^n(\phi_0, z). \quad (2.5)$$

Comparing Eq. (2.3) with Eq. (2.5) we see

$$\tilde{C}_n(r) = C_n(\phi_0). \quad (2.6)$$

Coefficients C_n can be determined from the solution to the Balitsky-Kovchegov equation [36], in the saturation region. The numerical solution has been found in Ref. [51] for the simplified BFKL kernel in which only the leading twist contribution was taken into account:

$$N^{\text{BK}}(G_{\mathcal{P}}(\phi_0, z)) = a(1 - \exp(-G_{\mathcal{P}}(\phi_0, z))) + (1 - a) \frac{G_{\mathcal{P}}(\phi_0, z)}{1 + G_{\mathcal{P}}(\phi_0, z)}, \quad (2.7)$$

with $a = 0.65$. Eq. (2.7) is a convenient parameterization of the numerical solution, with an accuracy of better than 5%. Having C_n we can calculate the Green function of the dressed BFKL Pomeron using Eq. (2.2), and the property of the BFKL Pomeron exchange:

$$\begin{aligned} \frac{\alpha_S^2}{4\pi} G_{\mathcal{P}}(Y - 0, r, R; b) = \\ \int d^2 r' d^2 b' d^2 r'' d^2 b'' G_{\mathcal{P}}(Y - Y', r, r', \vec{b} - \vec{b}') G_{\mathcal{P}}(Y' r'', R, \vec{b}'') A_{\text{dipole-dipole}}^{\text{BA}}(r', r'', \vec{b}' - \vec{b}') \end{aligned} \quad (2.8)$$

Carrying out the integrations in Eq. (2.2), we obtain the Green function of the dressed Pomeron in the following form:

$$\begin{aligned} G^{\text{dressed}}(T) &= a^2(1 - \exp(-T)) + 2a(1 - a) \frac{T}{1 + T} + (1 - a)^2 G(T) \\ \text{with } G(T) &= 1 - \frac{1}{T} \exp\left(\frac{1}{T}\right) \Gamma\left(0, \frac{1}{T}\right) \end{aligned} \quad (2.9)$$

where $\Gamma(s, z)$ is the upper incomplete gamma function (see Ref. [54] formula **8.35**), and T denotes the BFKL Pomeron in the vicinity of the saturation scale (see Eq. (2.4))

$$T(r_{\perp}, Y = \ln(s/s_0), b) = \phi_0 (r_{\perp}^2 Q_s^2(Y, b))^{\bar{\gamma}} \quad (2.10)$$

The Green function of Eq. (2.9) depends on the size of the dipoles, and we will use it for discussing the hard processes. In our analysis of the soft interaction we fixed $r = 1/m$, and m was a fitting parameter.

2.2 Phenomenology: assumptions and new small parameters

Unfortunately, due to the embryonic stage of theoretical understanding of the confinement of quarks and gluons, it is necessary to use pure phenomenological ideas to fix two major problems in high energy scattering: the structure of hadrons, and the large impact parameter behavior of the scattering amplitude [55]. The main idea to correct the large impact parameter behaviour, is to assume that the saturation momentum has the following dependence on the impact parameter b :

$$Q_s^2(b, Y) = Q_{0s}^2(b, Y_0) e^{\lambda(Y - Y_0)} \quad (2.11)$$

with

$$Q_{0s}^2(b, Y_0) = (m^2)^{1-1/\bar{\gamma}} (S(b, m))^{1/\bar{\gamma}} \quad S(b, m) = \frac{m^2}{2\pi} e^{-mb} \quad \text{and } \bar{\gamma} = 0.63 \quad (2.12)$$

We have introduced a new phenomenological parameter m to describe the large b behaviour. The Y dependence as well as r^2 dependence, can be found from CGC/saturation approach [31], since ϕ_0 and λ

can be calculated in the leading order of perturbative QCD. However, since the higher order corrections turn out to be large [56], we treat them as parameters to be fitted. m is a non-perturbative parameter, which determines the typical sizes of dipoles within the hadrons. In Table 1, we show that from the fit, $m = 5.25$ GeV, supporting our main assumption that we can apply the BFKL Pomeron calculus, based on perturbative QCD, to the soft interaction since $m \gg \mu_{soft}$, where μ_{soft} is the scale of soft interaction, which is of the order of the mass of pion or Λ_{QCD} .

The idea to absorb the non-perturbative b dependence into the saturation scale, stems both from the success of this idea in the description of the hard processes in framework of the saturation model [57–77], and from the semi-classical solution to the BK equation [78], as well as from the analytical solution deep in the saturation domain [79].

The second unsolved problem for which we need a phenomenological input, is the structure of the scattering hadrons. We use a two channel model, which allows us to calculate the diffractive production in the region of small masses. In this model, we replace the rich structure of the diffractively produced states, by a single state with the wave function ψ_D , a la Good-Walker [80]. The observed physical hadronic and diffractive states are written in the form

$$\psi_h = \alpha \Psi_1 + \beta \Psi_2; \quad \psi_D = -\beta \Psi_1 + \alpha \Psi_2; \quad \text{where} \quad \alpha^2 + \beta^2 = 1; \quad (2.13)$$

Functions ψ_1 and ψ_2 form a complete set of orthogonal functions $\{\psi_i\}$ which diagonalize the interaction matrix T

$$A_{i,k}^{i'k'} = \langle \psi_i \psi_k | \mathbf{T} | \psi_{i'} \psi_{k'} \rangle = A_{i,k} \delta_{i,i'} \delta_{k,k'}. \quad (2.14)$$

The unitarity constraints take the form

$$2 \text{Im} A_{i,k}(s, b) = |A_{i,k}(s, b)|^2 + G_{i,k}^{in}(s, b), \quad (2.15)$$

where $G_{i,k}^{in}$ denotes the contribution of all non diffractive inelastic processes, i.e. it is the summed probability for these final states to be produced in the scattering of a state i off a state k . In Eq. (2.15) $\sqrt{s} = W$ denotes the energy of the colliding hadrons, and b the impact parameter. A simple solution to Eq. (2.15) at high energies, has the eikonal form with an arbitrary opacity $\Omega_{i,k}$, where the real part of the amplitude is much smaller than the imaginary part.

$$A_{i,k}(s, b) = i (1 - \exp(-\Omega_{i,k}(s, b))), \quad (2.16)$$

$$G_{i,k}^{in}(s, b) = 1 - \exp(-2\Omega_{i,k}(s, b)). \quad (2.17)$$

Eq. (2.17) implies that $P_{i,k}^S = \exp(-2\Omega_{i,k}(s, b))$, is the probability that the initial projectiles (i, k) reach the final state interaction unchanged, regardless of the initial state re-scatterings.

The first approach is to use the eikonal approximation for Ω in which

$$\Omega_{i,k}(r_\perp, Y - Y_0, b) = \int d^2b' d^2b'' g_i(\vec{b}', m_i) G^{\text{dressed}}\left(T\left(r_\perp, Y - Y_0, \vec{b}''\right)\right) g_k(\vec{b} - \vec{b}' - \vec{b}'', m_k) \quad (2.18)$$

where m_i denote the masses, which is introduced phenomenologically to determine the b dependence of g_i (see below).

We propose a more general approach, which takes into account the new small parameters, that are determined by fitting to the experimental data (see Table 1 and Fig. 1 for notation):

$$G_{3P}/g_i(b=0) \ll 1; \quad m \gg m_1 \text{ and } m_2 \quad (2.19)$$

The second equation in Eq. (2.19) leads to the fact that b'' in Eq. (2.18) is much smaller than b and b' , therefore, Eq. (2.18) can be re-written in a simpler form

$$\begin{aligned} \Omega_{i,k}(r_\perp, Y - Y_0, b) &= \left(\int d^2 b'' G^{\text{dressed}} \left(T(r_\perp, Y - Y_0, \vec{b}'') \right) \right) \int d^2 b' g_i(\vec{b}') g_k(\vec{b} - \vec{b}') \\ &= \tilde{G}^{\text{dressed}}(r_\perp, Y - Y_0) \int d^2 b' g_i(\vec{b}') g_k(\vec{b} - \vec{b}') \end{aligned} \quad (2.20)$$

Using the first small parameter of Eq. (2.19), we see that the main contribution stems from the net diagrams shown in Fig. 1-b. The sum of these diagrams [25] leads to the following expression for $\Omega_{i,k}(s, b)$

$$\Omega(r, Y - Y_0; b) = \int d^2 b' \frac{g_i(\vec{b}') g_k(\vec{b} - \vec{b}') \tilde{G}^{\text{dressed}}(r, Y - Y_0)}{1 + G_{3P} \tilde{G}^{\text{dressed}}(r, Y - Y_0) [g_i(\vec{b}') + g_k(\vec{b} - \vec{b}')]}; \quad (2.21)$$

$$g_i(b) = g_i S_p(b; m_i); \quad (2.22)$$

where

$$S_p(b, m_i) = \frac{1}{4\pi} m_i^3 b K_1(m_i b) \xrightarrow{\text{Fourier image}} \frac{1}{(1 + Q_T^2/m_i^2)^2} \quad (2.23)$$

$$\tilde{G}^{\text{dressed}}(r, Y - Y_0) = \int d^2 b G^{\text{dressed}}(T(r, Y - Y_0, b)) \quad (2.24)$$

where $T(r, Y - Y_0, b)$ is given by Eq. (2.10).

The impact parameter dependence of $S_p(b, m_i)$ is purely phenomenological, however, Eq. (2.23) which has a form of the electromagnetic proton form factor, leads to the correct ($\exp(-\mu b)$) behavior at large b [82], and has correct behavior at large Q_T , which has been calculate in the framework of perturbative QCD [83]. We wish to draw the reader's attention to the fact that m_1 and m_2 are the two dimensional scales in a hadron, which in the framework of the constituent quark model, we assign to the size of the hadron ($R_h \propto 1/m_1$), and the size of the constituent quark ($R_Q \propto 1/m_2$).

Note that $\tilde{G}^{\text{dressed}}(Y - Y_0)$ does not depend on b . In all previous formulae, the value of the triple BFKL Pomeron vertex is known: $G_{3P} = 1.29 \text{ GeV}^{-1}$.

For further discussion, we introduce the notation

$$N^{BK}(G_{IP}^i(r_\perp, Y, b)) = a (1 - \exp(-G_{IP}^i(r_\perp, Y, b))) + (1 - a) \frac{G_{IP}^i(r_\perp, Y, b)}{1 + G_{IP}^i(r_\perp, Y, b)}, \quad (2.25)$$

model	λ	ϕ_0 (GeV^{-2})	g_1 (GeV^{-1})	g_2 (GeV^{-1})	m (GeV)	m_1 (GeV)	m_2 (GeV)	β
I(soft int.)	0.38	0.0019	110.2	11.2	5.25	0.92	1.9	0.58
II:(soft + DIS)	0.38	0.0022	96.9	20.96	5.25	0.86	1.76	0.66

Table 1: Fitted parameters of the model. Fit I: parameters for the soft interaction at high energy are taken from Ref. [25]. The additional parameters for DIS were found by fitting to the F_2 structure function (see below). Fit II: joint fit to the soft interaction data at high energy and the DIS data.

with $a = 0.65$. Eq. (2.25) is an analytical approximation to the numerical solution for the BK equation [51]. $G_{\mathcal{P}}^i(r_{\perp}, Y; b) = g_i(b) \tilde{G}^{\text{dressed}}(r_{\perp}, Y - Y_0)$. We recall that the BK equation sums the ‘fan’ diagrams.

2.3 Results of the fit

In this paper we make two fits. In the first one (fit I in Table 1 and Table 3) we do not change the parameters that govern the soft interactions in our model, and are shown in Table 1. The additional parameters that we need for the description of the deep inelastic data, and which we will discuss in the next section (see Table 3), were fitted using the HERA data on the deep inelastic structure function F_2 . The second fit, is a joint fit to the soft strong interaction data and the DIS data. In Fig. 2 we show the results of our model compared with the HERA data. The model predictions are in accord with the data for $0.85 \leq Q^2 \leq 27 GeV^2$, while for higher values of Q^2 and of x , the model values are slightly larger than the data.

In Table 2 we present our predictions for the soft interaction observables, in general the values obtained in the model for the soft interactions agree with the published LHC data, as well as the new preliminary TOTEM values at $W = 2.7, 7, 8, 13$ TeV (see Ref. [81]). We are in very good agreement with the data for σ_{tot} , σ_{el} and B_{el} . Regarding σ_{sd} and σ_{dd} , a problem exists when attempting to compare with the experimental results. This is due to the difficulties of measuring diffractive events at LHC energies, the different experiments have different cuts on the values of the diffractive mass measured, making it problematic when attempting to compare the model predictions with the experimental results.

In Table 2 we show the results of the two fits, the results are close to one another, the main difference shows up only at high energies. Indeed, in fit I the cross section for single diffraction is equal to 14.9 mb, while in fit II this value is smaller (13.1 mb). The smaller value of the diffraction cross sections is closer to TOTEM and CMS data.

3. Deep inelastic scattering

3.1 Generalities

In this section, we compare our amplitude with the experimental data on deep inelastic scattering (DIS).

W (TeV)	σ_{tot} (mb)	σ_{el} (mb) (mb)	B_{el} (GeV^{-2})	single σ_{sd}^{smd} (mb)	diffraction σ_{sd}^{lmd} (mb)	double σ_{dd}^{smd} (mb)	diffraction σ_{dd}^{lmd} (mb)
0.576	62.3(60.7)	12.9(13.1)	15.2(15.17)	5.64(4.12)	1.85(1.79)	0.7(0.39)	0.46 (0.50)
0.9	69.2(68.07)	15(15.05)	16(15.95)	6.25(4.67)	2.39(2.35)	0.77(0.46)	0.67(0.745)
1.8	79.2(78.76)	18.2(19.1)	17.1(17.12)	7.1(5.44)	3.35(3.28)	0.89(0.56)	1.17 (1.30)
2.74	85.5(85.44)	20.2(21.4)	17.8(17.86)	7.6(5.91)	4.07(4.02)	0.97(0.63)	1.62(1.79)
7	99.8(100.64)	25(26.7)	19.5(19.6)	8.7(6.96)	6.2(6.17)	1.15(0.814)	3.27(3.67)
8	101.8(102.8)	25.7(27.4)	19.7(19.82)	8.82(7.1)	6.55(6.56)	1.17(0.841)	3.63(4.05)
13	109.3(111.07)	28.3(30.2)	20.6(20.74)	9.36(7.64)	8.08(8.11)	1.27(0.942)	5.11(5.74)
14	110.5(111.97)	28.7(30.6)	20.7(20.88)	9.44(7.71)	8.34(8.42)	1.27(0.96)	5.4(6.06)
57	131.7(134.0)	36.2(38.5)	23.1(23.0)	10.85(9.15)	15.02(15.01)	1.56(1.26)	13.7(15.6)

Table 2: The values of cross sections versus energy. σ_{sd}^{smd} and σ_{dd}^{smd} denote the cross sections for diffraction dissociation in the small mass region, for single and double diffraction, which stem from the Good-Walker mechanism. While σ_{sd}^{lmd} and σ_{dd}^{lmd} denote high mass diffraction, coming from the dressed Pomeron contributions. The predictions of fit II, are shown in brackets.

In the framework of our approach, the observables of DIS can be re-written using

$$N_{T,L}(Q, Y; b) = \int \frac{d^2r}{4\pi} \int_0^1 dz |\Psi_{T,L}^{\gamma^*}(Q, r, z)|^2 N(r, Y; b) \quad (3.1)$$

where $Y = \ln(1/x_{Bj})$ and x_{Bj} is the Bjorken x . z is the fraction of energy carried by quark. Q is the photon virtuality. b denotes the impact parameter for the scattering of the colorless dipole of size r with the proton. $N(r, Y; b)$ is the scattering amplitude of this dipole, which in our model can be written in the following form:

$$N(r, Y; b) = \alpha^2 N_1^{BK} \left(g_1 S(b, m_1) \tilde{G}_P(r; Y) \right) + \beta^2 N_2^{BK} \left(g_2 S(b, m_2) \tilde{G}_P(r; Y) \right) \quad (3.2)$$

In Eq. (3.1) $|\Psi_{T,L}^{\gamma^*}(Q, r, z)|^2$ is the probability to find a dipole of size r in a photon with the virtuality Q , and with transverse or longitudinal polarization. The wave functions are known (see Ref. [31] and reference therein) and they are equal to the following expressions:

$$(\Psi^* \Psi)_T^{\gamma^*} = \frac{2N_c}{\pi} \alpha_{em} \sum_f e_f^2 \{ [z^2 + (1-z)^2] \epsilon^2 K_1^2(\epsilon r) + m_f^2 K_0^2(\epsilon r) \}, \quad (3.3)$$

$$(\Psi^* \Psi)_L^{\gamma^*} = \frac{8N_c}{\pi} \alpha_{em} \sum_f e_f^2 Q^2 z^2 (1-z)^2 K_0^2(\epsilon r), \quad (3.4)$$

where $\epsilon^2 = m_f^2 + z(1-z)Q^2$.

Finally, the physical observables take the form:

$$\sigma_{T,L}(Q, Y) = 2 \int d^2b N_{T,L}(Q, Y; b) \quad (3.5)$$

$$F_2(Q, Y) = \frac{Q^2}{4\pi^2\alpha_{\text{e.m.}}} \left\{ \sigma_T + \sigma_L \right\} \quad (3.6)$$

3.2 Modification to also include DIS

First, we need to include the mild violation of the geometric scaling behavior of the scattering amplitude. We use the same procedure as has been suggested in Res. [57–77]: we change $\bar{\gamma}$ in Eq. (2.10)

$$\bar{\gamma} = 1 - \gamma_{cr} \rightarrow 1 - \gamma_{cr} - \frac{1}{2\kappa\lambda Y} \ln(r^2 Q_s^2(b)) = 0.63 - \frac{1}{2\kappa\lambda Y} \ln(r^2 Q_s^2(b)) \quad (3.7)$$

where $\kappa = \chi''(\gamma_{cr})/\chi'(\gamma_{cr}) = 9.8$. $\chi(\gamma)$ is the BFKL kernel which has the following form

$$\chi(\gamma) = 2\psi(1) - \psi(\gamma) - \psi(1 - \gamma) \quad \text{while} \quad \frac{\chi(\gamma_{cr})}{1 - \gamma_{cr}} = \frac{d\chi(\gamma)}{d\gamma} \bigg|_{\gamma=\gamma_{cr}} \quad (3.8)$$

where $\psi(z) = d\Gamma(z)/dz$ is the Euler ψ -function (see Ref. [54] formula **8.360**).

Since we take into account the contribution of the heavy c -quark we introduce a correction due to large mass of this quark:

$$x_{Bj} \rightarrow x_{Bj} \left(\frac{1}{1 + \frac{4m_c^2}{Q^2}} \right) \quad \text{or} \quad Y_c = Y - \ln(1 + 4m_c^2/Q^2) \quad (3.9)$$

In describing the saturation phenomena and fitting the strong interaction data, we assumed that the QCD coupling is frozen at some value of momentum μ_{soft} . However, for DIS we take into account the running QCD coupling, replacing Eq. (3.6) by the following expression

$$F_2(Q, Y) = \frac{Q^2}{4\pi^2\alpha_{\text{e.m.}}} \left\{ \frac{\bar{\alpha}_S(Q^2)}{\bar{\alpha}_S(\mu^2)} \sigma^{\text{light q}}(Q, Y) + \frac{\bar{\alpha}_S(Q^2 + 4m_c^2)}{\bar{\alpha}_S(\mu^2)} \sigma^{\text{charm q}}(Q, Y_c) \right\} \quad (3.10)$$

where μ denotes the typical mass of the soft strong interaction $\mu \sim 1 \text{ GeV}$ and

$$\frac{\bar{\alpha}_S(Q^2)}{\bar{\alpha}_S(\mu^2)} = \frac{1}{1 + \beta \bar{\alpha}_S(\mu^2) \ln(Q^2/\mu^2)} \quad (3.11)$$

with $\beta = 3/4$.

We consider the strong interaction data for energies $W \geq 0.546 \text{ TeV}$, while the experimental data from HERA were measured for lower energies. Therefore, we need to include the contribution of the secondary Reggeons which give a substantial contribution [84].

$$\sigma_R(Q, Y) = \int \frac{d^2 r}{4\pi} \left\{ (\Psi^* \Psi)_T^{\gamma^*} + (\Psi^* \Psi)_L^{\gamma^*} \right\} A_R r^2 \left(\frac{Q^2}{x_{Bj} Q_0^2} \right)^{\alpha_R(0)-1} \quad (3.12)$$

with $Q_0 = 1 \text{ GeV}$.

The final equation for F_2 takes a form:

$$F_2(Q, Y) = \frac{Q^2}{4\pi^2 \alpha_{\text{e.m.}}} \left\{ \frac{\bar{\alpha}_S(Q^2)}{\bar{\alpha}_S(\mu^2)} \sigma^{\text{light q}}(Q, Y) + \frac{\bar{\alpha}_S(Q^2 + 4m_c^2)}{\bar{\alpha}_S(\mu^2)} \sigma^{\text{charm q}}(Q, Y_c) + \sigma_R(Q, Y) \right\} \quad (3.13)$$

3.3 The description of the HERA data

We introduce in Eq. (3.13), a set of new parameters for DIS: m_q -mass of the light quark, which we hope will be of the order of the constituent quark mass ($\sim 300 \text{ MeV}$), the mass of charm quark ($m_c = 1.2 \div 1.5 \text{ GeV}$), μ which we believe will be of the order of 1 GeV , and we introduce two new parameters A and $\alpha_R(0)$ for the secondary Reggeon contribution. For A there is only one restriction that at $x_{bj} = 4 \cdot 10^{-6}$ $\sigma_R^{\text{light q}} \leq 0.02 \sigma_{\text{tot}}$, while $\alpha_R(0) = 0.4 \div 0.6$.

model	$m_q(\text{GeV})$	$m_c(\text{GeV})$	$\alpha_S(\mu)$	$\mu(\text{GeV})$	$A(\text{GeV}^2)$	$\alpha_R(0)$
I	0.3	1.25	0.263	1.2	2.34	0.55
II	0.2	1.2	0.34	1.25	5.44	0.56

Table 3: Fitted parameters for DIS. The description of fit I and fit II is given in section 2.3, and in the caption of Table 1.

In Table 3 we display the parameters that were determined by fitting to the data, Fig. 2 shows the quality of our fit to the DIS HERA data.

We consider the fit shown in Fig. 2 to be in very good agreement with the experimental data, and to demonstrate that our model is able to describe the hard processes to within an accuracy of 5%.

4. Inclusive production

The cross section of the inclusive production is a very important observable for our estimates, since it indicates how well, we can describe the multi particle generation processes in our model. We have described the experimental data in our soft interaction model [26], we now recalculate using our generalization of the model, that we have discussed above. Ref. [65] showed that the CGC/saturation approach is able to describe the LHC data on inclusive production. In this section we re-visit these calculations, using our model, which we can now apply both to soft and to hard processes.

The expression for the inclusive cross section takes the form [31, 65, 86] (see Fig. 3 for notation)

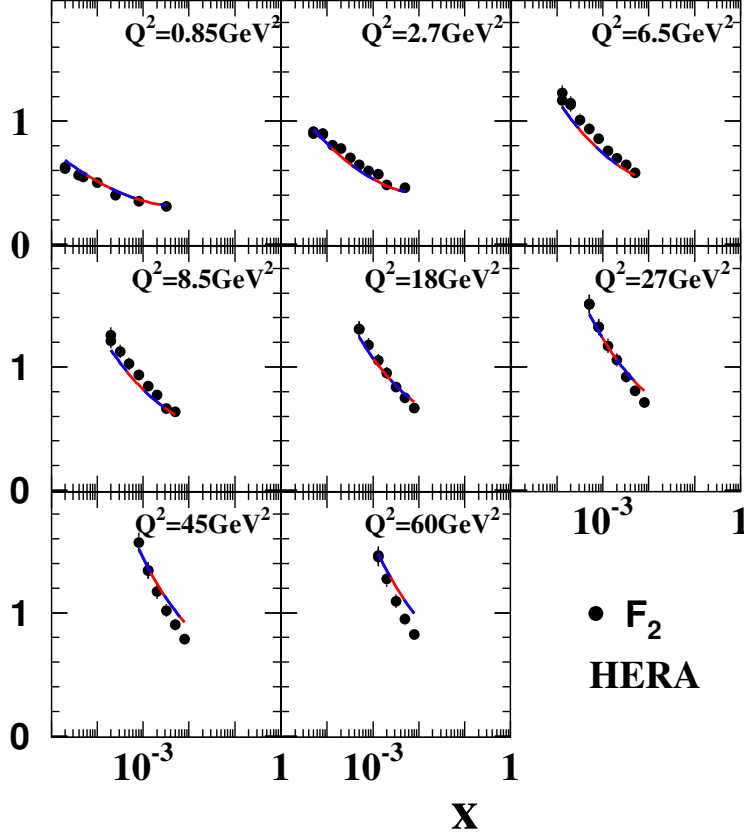


Figure 2: F_2 versus x at fixed Q . The red curve corresponds to fit I, while the blue one describes fit II. Data is taken from Ref. [33].

$$\frac{d\sigma}{dy d^2p_T} = \frac{2C_F}{\alpha_s(2\pi)^4} \frac{1}{p_T^2} \int d^2\vec{b} d^2\vec{B} d^2r e^{i\vec{p}_T \cdot \vec{r}} \nabla_T^2 N_G^{h_1}(Y - y; r; b) \nabla_T^2 N_G^{h_2}(y; r; |\vec{b} - \vec{B}|). \quad (4.1)$$

where the scattering amplitudes $N_G^{h_i}$ can be found from the dipole amplitude [86]

$$N_G^{h_i}(y_i; r; b) = 2N(y_i; r; b) - N^2(y_i; r; b), \quad (4.2)$$

and r denotes the dipole size. $C_F = (N_c^2 - 1)/2N_c$. For further discussion it is convenient to introduce two

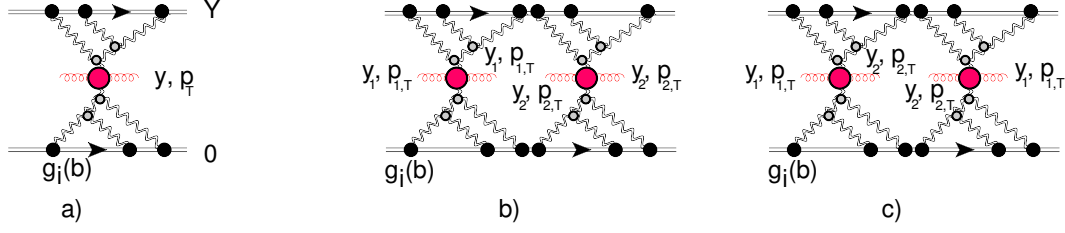


Figure 3: The generic Mueller diagrams [85] for single inclusive (Fig. 3-a) and for double inclusive (Fig. 3-b and Fig. 3-c) production. Fig. 3-b describes the double inclusive cross section, while Fig. 3-c shows the interference diagram for the Bose-Einstein correlation. For ease of drawing we take $y_1 = y_2$.

more observables

$$\begin{aligned} \frac{d\sigma_{i,j}}{dy d^2p_T d^2B} &= \frac{2C_F}{\alpha_s(2\pi)^4} \frac{1}{p_T^2} \int d^2b d^2r e^{i\vec{p}_T \cdot \vec{r}} \nabla_T^2 N_G^i(Y - y; r; b) \nabla_T^2 N_G^j(y; r; |\vec{b} - \vec{B}|); \\ \frac{d\sigma_{i,j}}{dy d^2p_T d^2B d^2b} &= \frac{2C_F}{\alpha_s(2\pi)^4} \frac{1}{p_T^2} \int d^2r e^{i\vec{p}_T \cdot \vec{r}} \nabla_T^2 N_G^i(Y - y; r; b) \nabla_T^2 N_G^j(y; r; |\vec{b} - \vec{B}|) \end{aligned} \quad (4.3)$$

where

$$N_G^i(y_i; r; b) = 2 N_i^{BK} \left(g_i S(b, m_i) \tilde{G}_P(r; y_i) \right) - \left(N_i^{BK} \left(g_i S(b, m_i) \tilde{G}_P(r; y_i) \right) \right)^2 \quad (4.4)$$

Taking for $N(y_i; r; b)$ in Eq. (4.2) the amplitude of Eq. (3.2) we obtain

$$\left. \frac{dN}{dy} \right|_{y=0} = \frac{1}{\sigma_{\text{NSD}}} \int d^2p_T \frac{d\sigma}{dy d^2p_T} \quad (4.5)$$

The values of $\sigma_{\text{NSD}} = \sigma_{\text{tot}} - \sigma_{\text{el}} - \sigma_{\text{single diffraction}}$ we take from the description of total and diffraction cross section in our model [25]. One can see that integral over p_T is logarithmical divergent at small p_T . As shown in Ref. [87] this divergence is regularized by the mass of produced gluon jet at $y = 0$. In Fig. 4 we plotted our estimates for $\left. \frac{dN}{dy} \right|_{y=0}$ using the value of this mass as was taken in Ref. [65] $m_{\text{jet}} = 350 \text{ MeV}$. The agreement with the experimental data is good and it gives us confidence that our model is able to discuss the typical process of many particle production. We do not need to discuss the rapidity distribution of the single inclusive cross section, since it has been discussed in Refs. [26, 65], where it is shown that this distribution agrees with the experimental data.

5. Azimuthal angle correlations

5.1 Double inclusive cross section

The Mueller diagram [85] for double inclusive cross section is shown in Fig. 3-b. Using Eq. (4.3) this cross section can be written in the form:

$$\Sigma_{i,j} \equiv \frac{d^2\sigma_{i,j}}{dy_1 d^2p_{1,T} dy_2 d^2p_{2,T}} = \int d^2B \frac{d\sigma}{dy_1 d^2p_{1,T} d^2B} \frac{d\sigma}{dy_2 d^2p_{2,T} d^2B} \quad (5.1)$$

$$\frac{d^2\sigma}{dy_1 d^2p_{1,T} dy_2 d^2p_{2,T}} = \alpha^4 \Sigma_{1,1} + 2\alpha^2 \beta^2 \Sigma_{1,2} + \beta^4 \Sigma_{2,2} \quad (5.2)$$

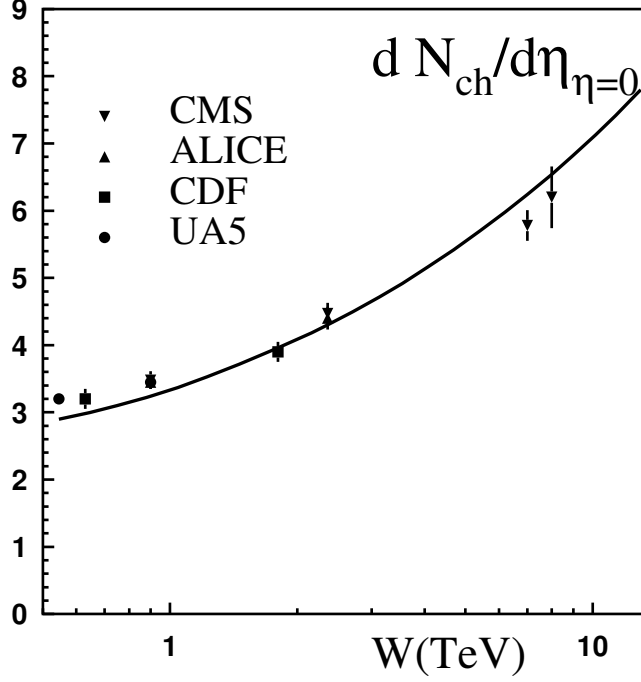


Figure 4: $\frac{dN}{dy} \Big|_{y=0}$ versus energy W . The experimental data are taken from Refs. [88–90] and Ref. [91]

We can re-write Eq. (5.1) in a different form if we introduce

$$I_i^G(y, r, Q_T) = \int d^2b e^{i\vec{Q}_T \cdot \vec{r}} \nabla_T^2 N_G^i(Y - y; r; b) \quad (5.3)$$

Note, that \vec{Q}_T denotes the transverse momentum carried by the BFKL Pomeron, which emits gluons with momentum $\vec{p}_{1,T}$ or $\vec{p}_{2,T}$.

Plugging Eq. (5.3) in Eq. (5.1) the expression for the double inclusive cross section takes the form

$$\begin{aligned} \frac{d^2\sigma_{i,j}}{dy_1 d^2p_{1,T} dy_2 d^2p_{2,T}} &= \frac{2C_F}{\alpha_s(2\pi)^4} \frac{1}{p_{1,T}^2} \frac{2C_F}{\alpha_s(2\pi)^4} \frac{1}{p_{2,T}^2} \int d^2r_1 e^{i\vec{p}_{1,T} \cdot \vec{r}_1} \int d^2r_2 e^{i\vec{p}_{2,T} \cdot \vec{r}_2} \\ &\times \int \frac{d^2Q_T}{(2\pi)^2} I_i^G(Y - y_1, r_1, Q_T) I_i^G(Y - y_2, r_2, Q_T) I_j^G(y_1, r_1, Q_T) I_j^G(y_2, r_2, Q_T) \end{aligned} \quad (5.4)$$

Therefore, using either Eq. (5.1) or Eq. (5.4) and the decomposition of Eq. (5.2), one can calculate the double inclusive cross section.

5.2 Bose-Einstein correlation: energy dependence

The double inclusive cross section of two identical gluons has the following general form:

$$\frac{d^2\sigma}{dy_1 dy_2 d^2p_{T1} d^2p_{T2}} (\text{identical gluons}) = \frac{d^2\sigma}{dy_1 dy_2 d^2p_{T1} d^2p_{T2}} (\text{different gluons}) \left(1 + C(L_c |\vec{p}_{T2} - \vec{p}_{T1}|) \right) \quad (5.5)$$

where $C(L_c |\vec{p}_{T2} - \vec{p}_{T1}|)$ denotes the correlation function, and L_c the correlation length. The first term in Eq. (5.5) is given by Eq. (5.1) or Eq. (5.4), while the second term describes the interference diagram for the identical gluons (see Fig. 3-c and Refs. [17, 32] for details). The expression for the interference term is more transparent in momentum representation, where it has the form

$$\begin{aligned} \frac{d^2\sigma_{i,j} (\text{interference contribution})}{dy_1 dy_2 d^2p_{T1} d^2p_{T2}} &= \frac{1}{N_c^2 - 1} \frac{2C_F}{\alpha_s(2\pi)^4} \frac{1}{p_{1,T}^2} \frac{2C_F}{\alpha_s(2\pi)^4} \frac{1}{p_{2,T}^2} \int d^2r_1 e^{i\vec{p}_{1,T} \cdot \vec{r}_1} \int d^2r_2 e^{i\vec{p}_{2,T} \cdot \vec{r}_2} \\ &\times \left\{ \int \frac{d^2Q_T}{(2\pi)^2} I_i^G(Y - y_1, r_1, Q_T) I_i^G(Y - y_2, r_2, Q_T) I_j^G\left(y_1, r_1, \vec{Q}_T - \vec{p}_{12,T}\right) I_j^G\left(y_2, r_2, \vec{Q}_T - \vec{p}_{12,T}\right) \right. \\ &= \int \frac{d^2Q'_T}{(2\pi)^2} I_i^G\left(Y - y_1, r_1, \vec{Q}'_T + \frac{1}{2}\vec{p}_{12,T}\right) I_i^G\left(Y - y_2, r_2, \vec{Q}'_T + \frac{1}{2}\vec{p}_{12,T}\right) \\ &\times \left. I_j^G\left(y_1, r_1, \vec{Q}_T - \frac{1}{2}\vec{p}_{12,T}\right) I_j^G\left(y_2, r_2, \vec{Q}_T - \frac{1}{2}\vec{p}_{12,T}\right) \right\} \quad (5.6) \end{aligned}$$

Eq. (5.6) takes into account that the lower BFKL Pomerons in Fig. 3-c, carry momenta $\vec{Q}_T - \vec{p}_{12,T}$, where $\vec{p}_{12,T} \equiv \vec{p}_{1,T} - \vec{p}_{2,T}$.

Eq. (5.6) can be re-written in the impact parameter representation using Eq. (4.3)

$$\begin{aligned} \frac{d^2\sigma_{i,j}}{dy_1 dy_2 d^2p_{T1} d^2p_{T2}} (\text{interference contribution}) &= \\ \frac{1}{N_c^2 - 1} \int d^2\vec{b} e^{i\vec{p}_{12,T} \cdot \vec{b}} \int d^2B' d^2b \frac{d\sigma_{i,j}}{dy d^2p_T d^2B d^2b} \left(\vec{b} + \frac{1}{2}\vec{b}, \vec{B}' + \frac{1}{2}\vec{b} \right) \frac{d\sigma_{i,j}}{dy d^2p_T d^2B d^2b} \left(\vec{b} - \frac{1}{2}\vec{b}, \vec{B}' - \frac{1}{2}\vec{b} \right) \end{aligned} \quad (5.7)$$

Finally, using the decomposition of Eq. (5.2), we can calculate the correlation function. In Fig. 5 we show the calculated correlation function

$$C(L_c |\vec{p}_{T2} - \vec{p}_{T1}|) = \frac{\frac{d^2\sigma}{dy_1 dy_2 d^2p_{T1} d^2p_{T2}} (\text{interference contribution})}{\frac{d^2\sigma}{dy_1 dy_2 d^2p_{T1} d^2p_{T2}} (\text{different gluons})} \quad (5.8)$$

From this figure we note that the correlation function does not depend on energy. This is an expected result. Indeed, the production of two parton showers, which is taken into account in Fig. 3-b and Fig. 3-c, leads to the correlation function, which does not depend on $y_{12} = |y_1 - y_2|$ (long range rapidity correlations(LRC)). This happens in our approach where the structure of one parton shower cannot be reduced to the exchange of the one BFKL Pomeron. Fig. 5 illustrates that the dependence on energy also cancels in the ratio of Eq. (5.8).

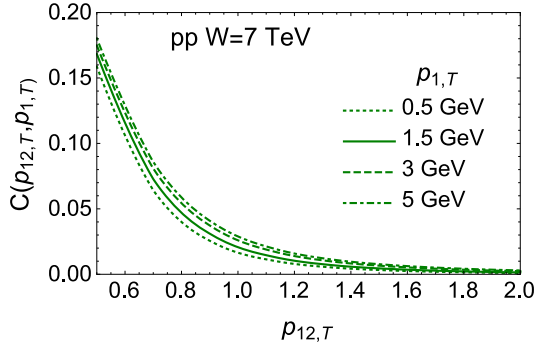


Fig. 5-a

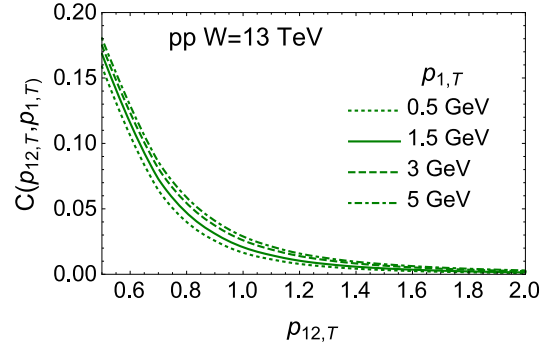


Fig. 5-b

Figure 5: Correlation function $C(L_c|\vec{p}_{T2} - \vec{p}_{T1}|)$ versus $\vec{p}_{12,T} \equiv \vec{p}_{1,T} - \vec{p}_{2,T}$ at different values of $p_{1,T}$ and energies $W = 7 \text{ TeV}$ (Fig. 5-a) and $W = 13 \text{ TeV}$ (Fig. 5-b).

5.3 Bose-Einstein correlation: values of v_n and its multiplicity dependence

We first introduce v_n , that can be defined in terms of the following representation of the double inclusive cross section

$$\frac{d^2\sigma}{dy_1 dy_2 d^2p_{T1} d^2p_{T2}} \propto 1 + 2 \sum_n v_{n,n}(p_{T1}, p_{T2}) \cos(n\varphi) \quad (5.9)$$

where φ is the angle between \vec{p}_{T1} and \vec{p}_{T2} . v_n is determined from $v_{n,n}(p_{T1}, p_{T2})$

$$1. \quad v_n(p_T) = \sqrt{v_{n,n}(p_T, p_T)}; \quad 2. \quad v_n(p_T) = \frac{v_{n,n}(p_T, p_T^{\text{Ref}})}{\sqrt{v_{n,n}(p_T^{\text{Ref}}, p_T^{\text{Ref}})}}; \quad (5.10)$$

Eq. (5.10)-1 and Eq. (5.10)-2 depict two methods of how the values of v_n have been extracted from the experimentally measured $v_{n,n}(p_{T1}, p_{T2})$. Where p_T^{Ref} denotes the momentum of the reference trigger. These two definitions are equivalent if $v_{n,n}(p_{T1}, p_{T2})$ can be factorized as $v_{n,n}(p_{T1}, p_{T2}) = v_n(p_{T1}) v_n(p_{T2})$. In this paper we use Eq. (5.10)-1 definition.

Taking into account Eq. (5.8) and Eq. (5.9) we obtain

$$v_{n,n} = \frac{\int_0^{2\pi} d\varphi C\left(2p_T \sin\left(\frac{1}{2}\varphi\right)\right) \cos(n\varphi)}{2\pi C(p_{12,T}=0) + \int_0^{2\pi} d\varphi C\left(2p_T \sin\left(\frac{1}{2}\varphi\right)\right) \cos(n\varphi)}; \quad v_n = \sqrt{v_{n,n}}; \quad (5.11)$$

Eq. (5.11) gives the prescription for the calculation of v_n that is measured as a sum of the events with all possible multiplicities of the secondary hadrons. However, in practice, only events with multiplicities larger than $2\bar{n}$, where \bar{n} is the average multiplicity which are measured in single inclusive experiments. Fig. 6 shows our calculations for $W = 13 \text{ TeV}$.

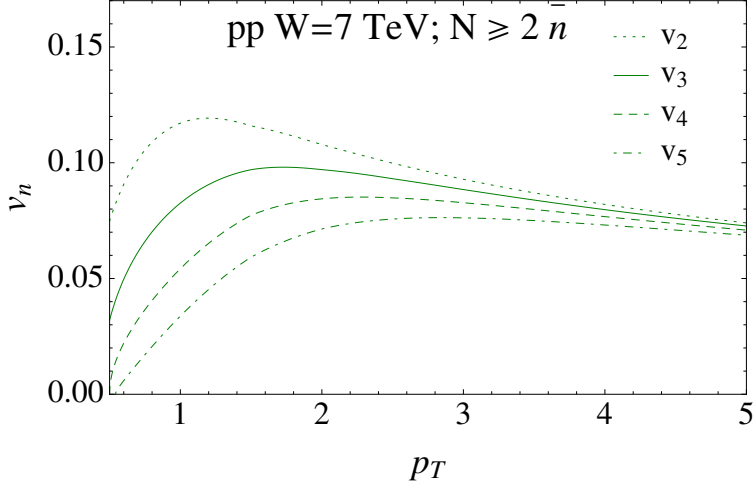


Figure 6: v_n versus p_T for the proton-proton scattering at $W = 7 \text{ TeV}$.

The dependence of v_n on the multiplicity of the event has been discussed in Ref. [32]. Eq. (5.7) takes a different form:

$$\frac{d^2\sigma}{dy_1 dy_2 d^2p_{T1} d^2p_{T2}} (\text{interference contribution}) = \frac{1}{N_c^2 - 1} \int d^2\tilde{b} e^{i\vec{p}_{12,T} \cdot \vec{\tilde{b}}} \quad (5.12)$$

$$\times \int d^2B' d^2b \frac{d\sigma}{dy d^2p_T d^2B d^2b} \left(\vec{b} + \frac{1}{2}\vec{\tilde{b}}, \vec{B}' + \frac{1}{2}\vec{\tilde{b}} \right) \frac{d\sigma}{dy d^2p_T d^2B d^2b} \left(\vec{b} - \frac{1}{2}\vec{\tilde{b}}, \vec{B}' - \frac{1}{2}\vec{\tilde{b}} \right) \frac{\sigma^{(m)}(\vec{b} + \vec{B}')}{\sigma_0};$$

with

$$\frac{\sigma^{(m)}(\vec{b} + \vec{B}')}{\sigma_0} = \frac{\Gamma(m - 2, 2\Omega(Y, \vec{b} + \vec{B}'))}{\Gamma(m - 2)}; \quad (5.13)$$

where $\Omega(r = 1/mY, b)$ is given by Eq. (2.21). Eq. (5.12) describes the Bose-Einstein correlations in the event whose multiplicity is large than $5\bar{n}$ ($N \geq 5\bar{n}$), where \bar{n} is the average multiplicity.

Comparing Fig. 6 and Fig. 7 one can see that in the framework of our approach, v_n do not depend on the multiplicity of the event. This independence is in excellent agreement with the experimental data (see Ref. [9] and Fig. 8). Note, that v_n do not depend on N only for proton-proton scattering, while for hadron-nucleus collisions, such dependence is considerable.

Fig. 5 shows that the correlation length $L_c \approx 1/m_1$ (the typical momentum is about m_1). From Table 1, the technical reason for this is clear, since the component with such characteristic momentum makes the largest contribution. In more general language the correlation length depends on the non-perturbative hadron structure. In terms of the processes, this typical transverse momentum is responsible for diffractive scattering with the production of hadrons with small masses. Intuitively, we expect that diffractive production of large masses, which depend on the saturation scale, can lead to larger typical momenta (smaller correlation length). We will discuss these processes in the next section.

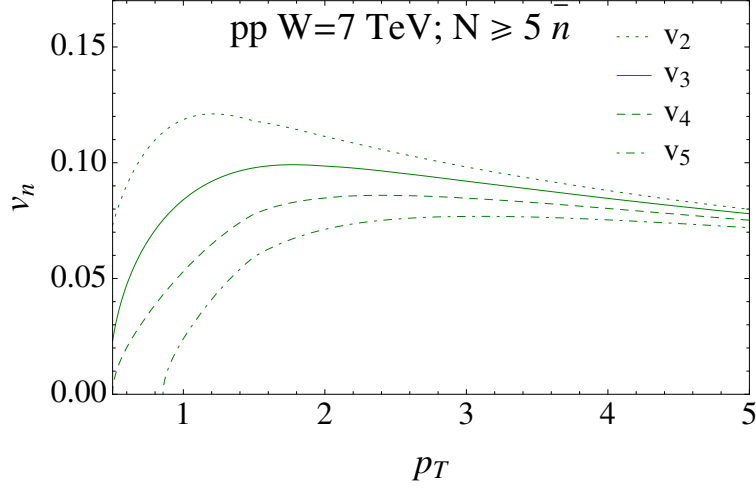


Figure 7: v_n versus p_T for proton-proton scattering at $W = 7 \text{ TeV}$ for the multiplicities $N \geq 5\bar{n}$.

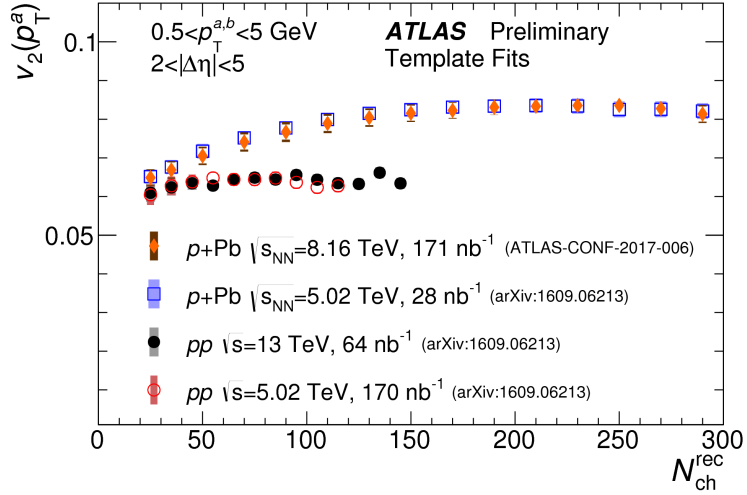


Figure 8: v_n versus multiplicities for hadron-hadron and hadron-nucleus interactions.

5.4 Bose-Einstein correlation: contribution of the semi-enhanced and enhanced diagrams (diffraction production of large masses)

In Fig. 9 we show the diagrams in our model that have not been taken into account. They correspond to single diffraction in the region of large masses (Fig. 9-a and Fig. 9-b), and to double diffraction in two bunches of particles with large masses (Fig. 9-c and Fig. 9-d).

One can see from Fig. 9, that all these diagrams contain the integration over y' . This integration is concentrated in the region $Y - y' \propto 1/\Delta_{\text{BFKL}}$, where Δ_{BFKL} is the intercept of the BFKL Pomeron. Performing this integration, we reduce the diagrams of the upper part of Fig. 9 to almost the same

expression as it was used in the previous section, but instead of $g_i(b)$ we need to insert the b -dependence of the triple Pomeron vertex, which in our model has the following form:

$$\Gamma_{3P} \propto e^{-2mb} \quad (5.14)$$

Bearing this in mind we can re-write $\frac{d\sigma}{dy d^2p_T d^2B d^2b}$ of Eq. (4.3) in the form

$$\begin{aligned} \frac{d\sigma_{i,j}}{dy d^2p_T d^2B d^2b} = & \quad (5.15) \\ \frac{e^{-mb}}{S(b, m_i)} \frac{m^2}{2\pi \sqrt{g_i(0)\lambda}} \frac{2C_F}{\alpha_s(2\pi)^4} \frac{1}{p_T^2} \int d^2r e^{i\vec{p}_T \cdot \vec{r}} \nabla_T^2 N_G^i(Y-y; r; b) \nabla_T^2 N_G^j(y; r; |\vec{b} - \vec{B}|) \end{aligned}$$

In Eq. (5.15) we restrict ourselves, by accounting only for interaction with the state $|1\rangle$, as $g_1(0) \gg g_2(0)$. Since in our model we have $m \gg m_1$, we can put $b = 0$. and reduce Eq. (5.15) to

$$\begin{aligned} \frac{d\sigma_{i,j}}{dy d^2p_T d^2B d^2b} = & \quad (5.16) \\ \frac{e^{-mb}}{S(b, m_i)} \frac{m^2}{2\pi \sqrt{g_i(0)\lambda}} \frac{2C_F}{\alpha_s(2\pi)^4} \frac{1}{p_T^2} \int d^2r e^{i\vec{p}_T \cdot \vec{r}} \nabla_T^2 N_G^i(Y-y; r; 0) \nabla_T^2 N_G^j(y; r; |\vec{B}|) \end{aligned}$$

for diagrams of Fig. 9-a and Fig. 9-b.

For the diagrams of Fig. 9-c and Fig. 9-d which correspond to double diffraction in large masses, we obtain

$$\begin{aligned} \frac{d\sigma_{i,j}}{dy d^2p_T d^2B d^2b} = & \quad (5.17) \\ \frac{e^{-mb-mB}}{S^2(b, m_i)} \frac{m}{2\pi g_i(0)\lambda} \frac{2C_F}{\alpha_s(2\pi)^4} \frac{1}{p_T^2} \int d^2r e^{i\vec{p}_T \cdot \vec{r}} \nabla_T^2 N_G^i(Y-y; r; 0) \nabla_T^2 N_G^j(y; r; 0) \end{aligned}$$

Plugging Eq. (5.16) and Eq. (5.17) into Eq. (5.2), we can calculate the double inclusive cross sections. Using them and plugging in Eq. (5.7) and Eq. (5.8), we obtain the correlation function and v_n . The result of these calculations is shown in Fig. 10. One can see that contributions of semi-enhanced and enhanced diagrams, which are closely related to the processes of diffractive production of large masses in single diffraction (LMD-SD) and in double diffraction (LSD-DD), increase the typical transverse momentum in v_n dependence, on transverse momenta.

Such behaviour is a direct consequence of the fact that typical momenta in the LSD contribution are of the order of Q_s , which is larger than m_1 and m_2 , which determine the hadron structure (see Fig. 11)

Comparing Fig. 10-a and Fig. 10-b, shows that the typical momentum for the sum of the diagrams, is larger than for the non-enhanced diagrams. Fig. 11 displays the dependence of $v_{n,n}$ in the semi-enhanced and enhanced diagrams. Comparing this figure with Fig. 10-b, we note that the contribution of these diagrams are larger than the non-enhanced one, leading to the explanation of p_T dependence in the experimental data of Fig. 12. Therefore, in our model the typical momentum is close to Q_s .

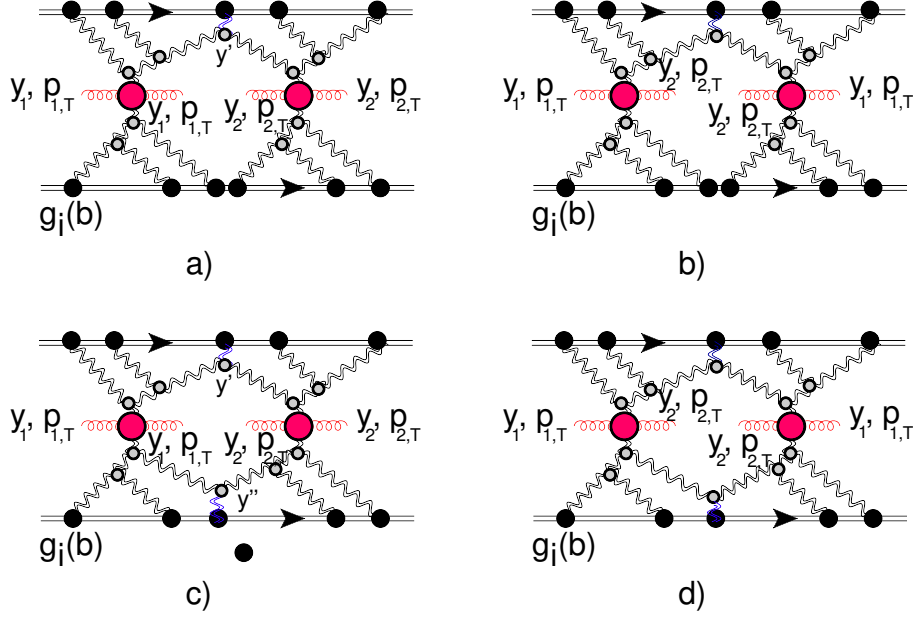


Figure 9: Semi-enhanced and enhanced diagrams: Fig. 9-a and Fig. 9-c show the cross sections of double inclusive productions; Fig. 9-b and Fig. 9-d describe the interference diagram that leads to Bose-Einstein correlations.

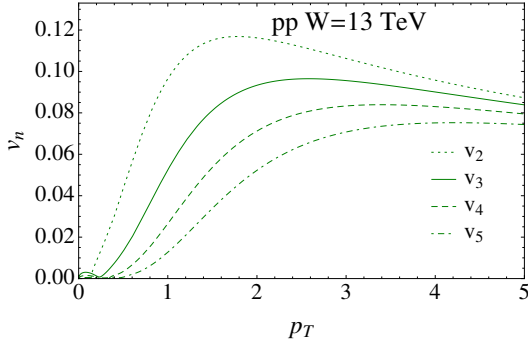


Fig. 10-a

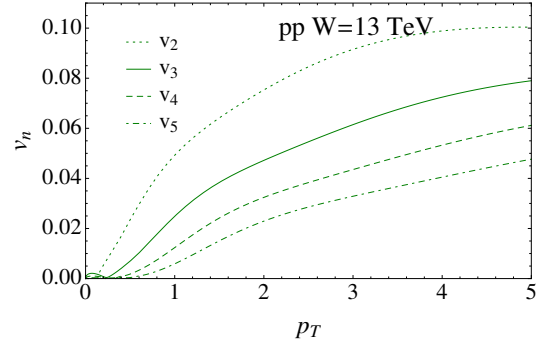


Fig. 10-b

Figure 10: v_n versus p_T at $W = 13 \text{ TeV}$ for non-enhanced diagram of Fig. 3 and sum of all contributions.

5.5 Comparison with the experiment

. In Fig. 12 and Fig. 13 we plot the experimental data [9] and the results of our calculations. One can see that we predict the values and p_T dependence of v_n which are in agreement with the experimental data. We wish to stress that we used Eq. (5.9)-1 for the estimates of the values of v_n , but one can see that our prediction for $v_{n,n}$ are also in accord with the data. As we have mentioned the semi-enhanced and enhanced diagrams are closely related to the processes of large mass diffraction. On the other hand, these processes give only about 30% contributions (see Table 2). Indeed, at $W = 13 \text{ TeV}$ $R_{\text{sd}}^{\text{lmd}} = \sigma_{\text{sd}}^{\text{lmd}} / (\sigma_{\text{el}} + \sigma_{\text{sd}}^{\text{smd}} + \sigma_{\text{dd}}^{\text{smd}}) = 0.26$ and $R_{\text{dd}}^{\text{lmd}} = \sigma_{\text{dd}}^{\text{lmd}} / (\sigma_{\text{el}} + \sigma_{\text{sd}}^{\text{smd}} + \sigma_{\text{dd}}^{\text{smd}}) = 0.16$.

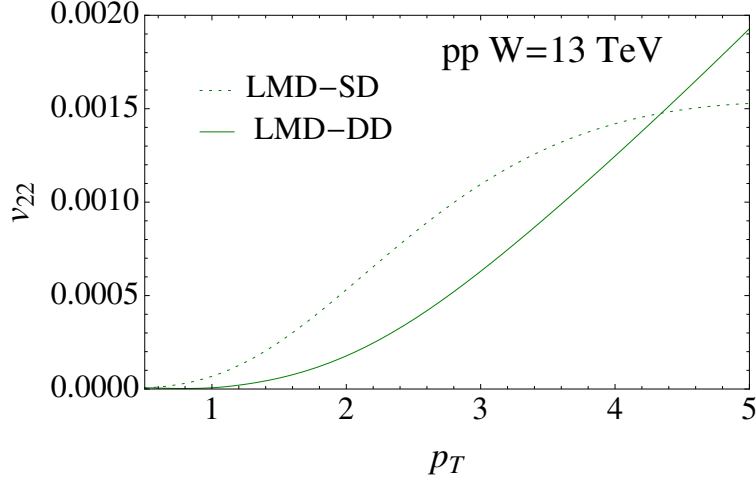


Figure 11: The contribution to v_{22} versus p_T at $W = 13 \text{ TeV}$ for large mass diffraction in single(LMD-SD) and in double (LMD-DD).

Such essential difference stems from the fact that the cross sections of diffractive production should be multiplied by the survival probability factor $\exp(-2\Omega(r, Y - Y_0, b))$ (see Eq. (2.21) and Ref. [25]). This factor results in substantial suppression of the diffractive production, however, it is absent in the double inclusive cross sections.

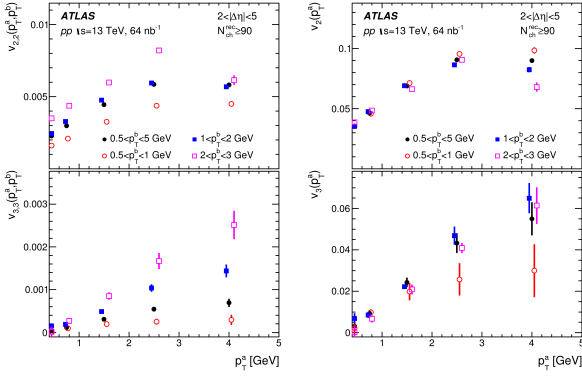


Figure 12: Experimental data for v_{nn} and v_n versus p_T at $W = 13 \text{ TeV}$. [9]

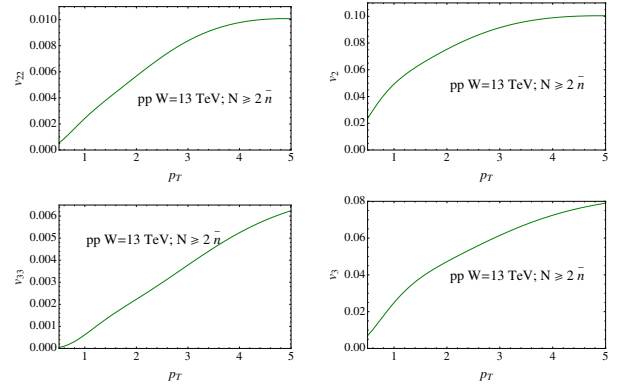


Figure 13: Our model for v_{nn} and v_n versus p_T at $W = 13 \text{ TeV}$.

6. Conclusions

In this paper we generalized our model to include the hard processes and presented our estimates for v_n for proton-proton collisions at high energy. Our main result can be formulated shortly: the model predicts Bose-Einstein correlations which lead to the values of v_n , that are in accord with the experimental values.

Our estimates are obtained from a model which is able to describe the typical soft observables for diffractive production, such as total and elastic cross section and cross section of diffraction production, inclusive cross sections, long range rapidity correlations and the deep inelastic F_2 structure function. In spite of being a phenomenological model which parameterizes the data rather than gives a theoretical interpretation, we believe that our model leads to reliable predictions for v_n at high energies. This belief is based not only on the fact that the model describes both diffractive processes and processes of the multi-particle generation, but also on the fact that it includes all that we know from CGC on the behavior of the scattering amplitude in the saturation region. We showed that the angular correlations do not depend on energy and multiplicity, in accord with the experimental data.

Therefore, before making extreme assumptions on proton-proton collisions, such as the production of quark-gluon plasma in the large multiplicity events, we need to explain what happens to the Bose-Einstein correlations which are so large, that they are able to describe the angular correlations in the proton-proton scattering, without taking into account interactions in the final state.

Acknowledgements We thank our colleagues at Tel Aviv University and UTFSM for encouraging discussions. Our special thanks go to Carlos Cantreras, Alex Kovner and Michel Lublinsky for elucidating discussions on the subject of this paper.

This research was supported by the BSF grant 2012124, by Proyecto Basal FB 0821(Chile) , Fondecyt (Chile) grant 1140842, and by CONICYT grant PIA ACT1406.

References

- [1] V. Khachatryan *et al.* [CMS Collaboration], arXiv:1510.03068 [nucl-ex]; JHEP **1009** (2010) 091 [arXiv:1009.4122 [hep-ex]]. arXiv:1510.03068 [nucl-ex].
- [2] J. Adams *et al.* [STAR Collaboration], Phys. Rev. Lett. **95** (2005) 152301 [nucl-ex/0501016].
- [3] B. Alver *et al.* [PHOBOS Collaboration], Phys. Rev. Lett. **104** (2010) 062301 [arXiv:0903.2811 [nucl-ex]].
- [4] H. Agakishiev *et al.* [STAR Collaboration], arXiv:1010.0690 [nucl-ex].
- [5] S. Chatrchyan *et al.* [CMS Collaboration], Phys. Lett. B **718** (2013) 795 [arXiv:1210.5482 [nucl-ex]]; V. Khachatryan *et al.* [CMS Collaboration], JHEP **1009** (2010) 091, [arXiv:1009.4122 [hep-ex]].
- [6] S. Chatrchyan *et al.* [CMS Collaboration], JHEP **1402** (2014) 088, [arXiv:1312.1845 [nucl-ex]]; Phys. Rev. C **89** (2014) no.4, 044906; [arXiv:1310.8651 [nucl-ex]]; “Centrality dependence of dihadron correlations and azimuthal anisotropy harmonics in PbPb collisions at $\sqrt{s_{NN}} = 2.76$ TeV,” Eur. Phys. J. C **72** (2012) 2012 [arXiv:1201.3158 [nucl-ex]]; JHEP **1402** (2014) 088 doi:10.1007/JHEP02(2014)088 [arXiv:1312.1845 [nucl-ex]].
- [7] J. Adam *et al.* [ALICE Collaboration], arXiv:1604.07663 [nucl-ex]; Phys. Rev. Lett. **116** (2016) no.13, 132302, [arXiv:1602.01119 [nucl-ex]]; L. Milano [ALICE Collaboration], Nucl. Phys. A **931** (2014) 1017, [arXiv:1407.5808 [hep-ex]]; Y. Zhou [ALICE Collaboration], J. Phys. Conf. Ser. **509** (2014) 012029, [arXiv:1309.3237 [nucl-ex]].

- [8] B. B. Abelev *et al.* [ALICE Collaboration], Phys. Rev. C **90** (2014) no.5, 054901, [arXiv:1406.2474 [nucl-ex]]; B. B. Abelev *et al.* [ALICE Collaboration], Phys. Lett. B **726** (2013) 164 doi:10.1016/j.physletb.2013.08.024 [arXiv:1307.3237 [nucl-ex]]; B. Abelev *et al.* [ALICE Collaboration], Phys. Lett. B **719** (2013) 29, [arXiv:1212.2001 [nucl-ex]].
- [9] M. Aaboud *et al.* [ATLAS Collaboration], “*Measurements of long-range azimuthal anisotropies and associated Fourier coefficients for pp collisions at $\sqrt{s} = 5.02$ and 13 TeV and p+Pb collisions at $\sqrt{s_{NN}} = 5.02$ TeV with the ATLAS detector,*” arXiv:1609.06213 [nucl-ex].
G. Aad *et al.* [ATLAS Collaboration], Phys. Rev. Lett. **116** (2016) 172301, [arXiv:1509.04776 [hep-ex]].
- [10] G. Aad *et al.* [ATLAS Collaboration], Phys. Rev. C **90** (2014) no.4, 044906; [arXiv:1409.1792 [hep-ex]]; B. Wosiek [ATLAS Collaboration], Annals Phys. **352** (2015) 117; G. Aad *et al.* [ATLAS Collaboration], Phys. Lett. B **725** (2013) 60, [arXiv:1303.2084 [hep-ex]].
- [11] B. Wosiek [ATLAS Collaboration], Phys. Rev. C **86** (2012) 014907, [arXiv:1203.3087 [hep-ex]].
- [12] E. M. Levin, M. G. Ryskin and S. I. Troian, Sov. J. Nucl. Phys. **23** (1976) 222 [Yad. Fiz. **23** (1976) 423]; A. Capella, A. Krzywicki and E. M. Levin, Phys. Rev. D **44** (1991) 704.
- [13] E. Gotsman, E. Levin and U. Maor, Phys. Rev. D **95**, no. 3, 034005 (2017) doi:10.1103/PhysRevD.95.034005 [arXiv:1604.04461 [hep-ph]].
- [14] A. Kovner and M. Lublinsky, Phys. Rev. D **83**, 034017 (2011), [arXiv:1012.3398 [hep-ph]].
- [15] Y. V. Kovchegov and D. E. Wertepny, Nucl. Phys. A **906** (2013) 50, [arXiv:1212.1195 [hep-ph]].
- [16] T. Altinoluk, N. Armesto, G. Beuf, A. Kovner and M. Lublinsky, Phys. Lett. B **752** (2016) 113, [arXiv:1509.03223 [hep-ph]]; T. Altinoluk, N. Armesto, G. Beuf, A. Kovner and M. Lublinsky, Phys. Lett. B **751** (2015) 448, [arXiv:1503.07126 [hep-ph]].
- [17] E. Gotsman and E. Levin, Phys. Rev. D **95** (2017) no.1, 014034 [arXiv:1611.01653 [hep-ph]].
- [18] A. Kovner, M. Lublinsky and V. Skokov, “*Exploring correlations in the CGC wave function: odd azimuthal anisotropy,*” arXiv:1612.07790 [hep-ph].
- [19] K. Dusling and R. Venugopalan, Phys. Rev. D **87** (2013) no.9, 094034, [arXiv:1302.7018 [hep-ph]] and reference therein.
- [20] A. Kovner and M. Lublinsky, Int. J. Mod. Phys. E **22**, 1330001 (2013), [arXiv:1211.1928 [hep-ph]] and references therein.
- [21] E. Gotsman, E. Levin and U. Maor, Eur. Phys. J. C **76** (2016) no.11, 607, arXiv:1607.00594 [hep-ph].
- [22] R. Hanbury Brown and R. Q. Twiss, Nature **178** (1956) 1046.
- [23] G. Goldhaber, W. B. Fowler, S. Goldhaber and T. F. Hoang, Phys. Rev. Lett. **3**, 181 (1959); G. I. Kopylov and M. I. Podgoretsky, Sov. J. Nucl. Phys. **15**, 219 (1972) [Yad. Fiz. **15**, 392 (1972)]; G. Alexander, Rept. Prog. Phys. **66** (2003) 481, [hep-ph/0302130].
- [24] E. Gotsman, E. Levin and U. Maor, Eur. Phys. J. C **75** (2015) 1, 18 [arXiv:1408.3811 [hep-ph]].
- [25] E. Gotsman, E. Levin and U. Maor, Eur. Phys. J. C **75** (2015) 5, 179 [arXiv:1502.05202 [hep-ph]].
- [26] E. Gotsman, E. Levin and U. Maor, Phys. Lett. B **746** (2015) 154 [arXiv:1503.04294 [hep-ph]].

- [27] E. Gotsman, E. Levin and U. Maor, Eur. Phys. J. C **75** (2015) 11, 518 [arXiv:1508.04236 [hep-ph]].
- [28] E. Gotsman, E. Levin and U. Maor, arXiv:1510.07249 [hep-ph].
- [29] E. Gotsman, E. Levin, U. Maor and S. Tapia, Phys. Rev. D **93** (2016) no.7, 074029 doi:10.1103/PhysRevD.93.074029 [arXiv:1603.02143 [hep-ph]].
- [30] E. Iancu, K. Itakura and L. McLerran, Nucl. Phys. A **708** (2002) 327, [hep-ph/0203137]; A. M. Stasto, K. J. Golec-Biernat and J. Kwiecinski, Phys. Rev. Lett. **86** (2001) 596, [hep-ph/0007192]; E. Levin and K. Tuchin, Nucl. Phys. B **573** (2000) 833, [hep-ph/9908317]. J. Bartels and E. Levin, Nucl. Phys. B **387** (1992) 617.
- [31] Yuri V Kovchegov and Eugene Levin, “*Quantum Chromodynamics at High Energies*”, Cambridge Monographs on Particle Physics, Nuclear Physics and Cosmology, Cambridge University Press, 2012 .
- [32] E. Gotsman and E. Levin, *Bose-Einstein correlations in perturbative QCD: v_n dependence on multiplicity*.
- [33] H. Abramowicz *et al.* [ZEUS Collaboration], Phys. Rev. D **93** (2016) no.9, 092002, [arXiv:1603.09628 [hep-ex]]; H. Abramowicz *et al.* [H1 and ZEUS Collaborations], Eur. Phys. J. C **75** (2015) no.12, 580, [arXiv:1506.06042 [hep-ex]].
- [34] L. McLerran and R. Venugopalan, Phys. Rev. **D49** (1994) 2233, 3352; **D50** (1994) 2225; **D53** (1996) 458; **D59** (1999) 09400.
- [35] A. H. Mueller, Nucl. Phys. B **415**, 373 (1994); Nucl. Phys. B **437** (1995) 107 [arXiv:hep-ph/9408245].
- [36] I. Balitsky, [arXiv:hep-ph/9509348]; *Phys. Rev.* **D60**, 014020 (1999) [arXiv:hep-ph/9812311]; Y. V. Kovchegov, *Phys. Rev.* **D60**, 034008 (1999), [arXiv:hep-ph/9901281].
- [37] J. Jalilian-Marian, A. Kovner, A. Leonidov and H. Weigert, *Phys. Rev.* **D59**, 014014 (1999), [arXiv:hep-ph/9706377]; *Nucl. Phys.* **B504**, 415 (1997), [arXiv:hep-ph/9701284]; J. Jalilian-Marian, A. Kovner and H. Weigert, *Phys. Rev.* **D59**, 014015 (1999), [arXiv:hep-ph/9709432]; A. Kovner, J. G. Milhano and H. Weigert, *Phys. Rev.* **D62**, 114005 (2000), [arXiv:hep-ph/0004014]; E. Iancu, A. Leonidov and L. D. McLerran, *Phys. Lett.* **B510**, 133 (2001); [arXiv:hep-ph/0102009]; *Nucl. Phys.* **A692**, 583 (2001), [arXiv:hep-ph/0011241]; E. Ferreira, E. Iancu, A. Leonidov and L. McLerran, *Nucl. Phys.* **A703**, 489 (2002), [arXiv:hep-ph/0109115]; H. Weigert, *Nucl. Phys.* **A703**, 823 (2002), [arXiv:hep-ph/0004044].
- [38] E. A. Kuraev, L. N. Lipatov, and F. S. Fadin, *Sov. Phys. JETP* **45**, 199 (1977); Ya. Ya. Balitsky and L. N. Lipatov, *Sov. J. Nucl. Phys.* **28**, 22 (1978).
- [39] L. N. Lipatov, Phys. Rep. **286** (1997) 131; Sov. Phys. JETP **63** (1986) 904 and references therein.
- [40] L. V. Gribov, E. M. Levin and M. G. Ryskin, Phys. Rep. **100** (1983) 1.
- [41] E. M. Levin and M. G. Ryskin, Phys. Rept. **189**, 267 (1990).
- [42] A. H. Mueller and J. Qiu, Nucl. Phys. **B268** (1986) 427.
- [43] A. H. Mueller and B. Patel, Nucl. Phys. **B425** (1994) 471.
- [44] J. Bartels, M. Braun and G. P. Vacca, Eur. Phys. J. **C40** (2005) 419 [arXiv:hep-ph/0412218]. J. Bartels and C. Ewerz, JHEP **9909** 026 (1999) [arXiv:hep-ph/9908454]. J. Bartels and M. Wusthoff, Z. Phys. **C6**, (1995) 157. J. Bartels, Z. Phys. **C60** (1993) 471.

- [45] M. A. Braun, Phys. Lett. **B632** (2006) 297 [arXiv:hep-ph/0512057]; Eur. Phys. J. **C16** (2000) 337 [arXiv:hep-ph/0001268]; Phys. Lett. **B483** (2000) 115 [arXiv:hep-ph/0003004]; Eur. Phys. J. **C33** (2004) 113 [arXiv:hep-ph/0309293]; **C6**, 321 (1999) [arXiv:hep-ph/9706373]. M. A. Braun and G. P. Vacca, Eur. Phys. J. **C6** (1999) 147 [arXiv:hep-ph/9711486].
- [46] Y. V. Kovchegov and E. Levin, Nucl. Phys. B **577** (2000) 221 [hep-ph/9911523].
- [47] E. Levin and M. Lublinsky, Nucl. Phys. A **763** (2005) 172 [arXiv:hep-ph/0501173]; Phys. Lett. B **607** (2005) 131 [arXiv:hep-ph/0411121]; Nucl. Phys. A **730** (2004) 191 [arXiv:hep-ph/0308279].
- [48] E. Levin, J. Miller and A. Prygarin, Nucl. Phys. **A806** (2008) 245, [arXiv:0706.2944 [hep-ph]].
- [49] T. Altinoluk, C. Contreras, A. Kovner, E. Levin, M. Lublinsky and A. Shulkin, Int. J. Mod. Phys. Conf. Ser. **25** (2014) 1460025; T. Altinoluk, N. Armesto, A. Kovner, E. Levin and M. Lublinsky, JHEP **1408** (2014) 007.
- [50] T. Altinoluk, A. Kovner, E. Levin and M. Lublinsky, JHEP **1404** (2014) 075 [arXiv:1401.7431 [hep-ph]].; T. Altinoluk, C. Contreras, A. Kovner, E. Levin, M. Lublinsky and A. Shulkin, JHEP **1309** (2013) 115.
- [51] E. Levin, JHEP **1311** (2013) 039 [arXiv:1308.5052 [hep-ph]].
- [52] A. H. Mueller and B. Patel, Nucl. Phys. **B425** (1994) 471. A. H. Mueller and G. P. Salam, Nucl. Phys. **B475**, (1996) 293. [arXiv:hep-ph/9605302]. G. P. Salam, Nucl. Phys. **B461** (1996) 512; E. Iancu and A. H. Mueller, Nucl. Phys. **A730** (2004) 460 [arXiv:hep-ph/0308315]; 494 [arXiv:hep-ph/0309276].
- [53] A. H. Mueller and D. N. Triantafyllopoulos, Nucl. Phys. B **640**, 331 (2002); [hep-ph/0205167].
- [54] I. Gradshteyn and I. Ryzhik, *Table of Integrals, Series, and Products*, Fifth Edition, Academic Press, London, 1994.
- [55] A. Kovner and U. A. Wiedemann, Phys. Rev. D **66**, 051502, 034031 (2002) [hep-ph/0112140, hep-ph/0204277]; Phys. Lett. B **551**, 311 (2003) [hep-ph/0207335].
- [56] V. A. Khoze, A. D. Martin, M. G. Ryskin and W. J. Stirling, Phys. Rev. D **70** (2004) 074013 [hep-ph/0406135]; D. N. Triantafyllopoulos, Nucl. Phys. B **648** (2003) 293 [hep-ph/0209121].
- [57] E. Iancu, K. Itakura and S. Munier, Phys. Lett. B **590** (2004) 199 [hep-ph/0310338].
- [58] K. J. Golec-Biernat and M. Wusthoff, Phys. Rev. D **60** (1999) 114023 [hep-ph/9903358]; Phys. Rev. D **59** (1998) 014017; [hep-ph/9807513].
- [59] J. Bartels, K. J. Golec-Biernat and H. Kowalski, Phys. Rev. D **66** (2002) 014001 [hep-ph/0203258].
- [60] H. Kowalski and D. Teaney, Phys. Rev. D **68** (2003) 114005 [hep-ph/0304189].
- [61] H. Kowalski, L. Motyka and G. Watt, Phys. Rev. D **74** (2006) 074016 [hep-ph/0606272].
- [62] H. Kowalski, T. Lappi and R. Venugopalan, Phys. Rev. Lett. **100** (2008) 022303 [arXiv:0705.3047 [hep-ph]].
- [63] H. Kowalski, T. Lappi, C. Marquet and R. Venugopalan, Phys. Rev. C **78** (2008) 045201 [arXiv:0805.4071 [hep-ph]].
- [64] G. Watt and H. Kowalski, Phys. Rev. D **78** (2008) 014016 [arXiv:0712.2670 [hep-ph]].
- [65] E. Levin and A. H. Rezaeian, Phys. Rev. D **82** (2010) 014022 [arXiv:1005.0631 [hep-ph]].
- [66] A. H. Rezaeian, Phys. Lett. B **718** (2013) 1058 [arXiv:1210.2385 [hep-ph]].
- [67] E. Levin and A. H. Rezaeian, Phys. Rev. D **83** (2011) 114001 [arXiv:1102.2385 [hep-ph]].

- [68] E. Levin and A. H. Rezaeian, Phys. Rev. D **82** (2010) 054003 [arXiv:1007.2430 [hep-ph]].
- [69] D. Boer, M. Diehl, R. Milner, R. Venugopalan, W. Vogelsang, D. Kaplan, H. Montgomery and S. Vigdor *et al.*, arXiv:1108.1713 [nucl-th].
- [70] T. Lappi and H. Mantysaari, Phys. Rev. C **83** (2011) 065202 [arXiv:1011.1988 [hep-ph]].
- [71] T. Toll and T. Ullrich, Phys. Rev. C **87** (2013) 2, 024913 [arXiv:1211.3048 [hep-ph]].
- [72] P. Tribedy and R. Venugopalan, Nucl. Phys. A **850** (2011) 136 [Nucl. Phys. A **859** (2011) 185] [arXiv:1011.1895 [hep-ph]].
- [73] P. Tribedy and R. Venugopalan, Phys. Lett. B **710** (2012) 125 [Phys. Lett. B **718** (2013) 1154] [arXiv:1112.2445 [hep-ph]].
- [74] A. H. Rezaeian, M. Siddikov, M. Van de Klundert and R. Venugopalan, PoS DIS **2013** (2013) 060 [arXiv:1307.0165 [hep-ph]]; Phys. Rev. D **87** (2013) 3, 034002 [arXiv:1212.2974].
- [75] A. H. Rezaeian and I. Schmidt, Phys. Rev. D **88** (2013) 074016 [arXiv:1307.0825 [hep-ph]].
- [76] C. Contreras, E. Levin, R. Meneses and I. Potashnikova, Phys. Rev. D **94** (2016) no.11, 114028; [arXiv:1607.00832 [hep-ph]].
- [77] C. Contreras, E. Levin and I. Potashnikova, Nucl. Phys. A **948** (2016) 1, [arXiv:1508.02544 [hep-ph]].
- [78] S. Bondarenko, M. Kozlov and E. Levin, Nucl. Phys. A **727** (2003) 139 [hep-ph/0305150].
- [79] E. Levin and K. Tuchin, Nucl. Phys. B **573** (2000) 833 doi:10.1016/S0550-3213(99)00825-1 [hep-ph/9908317].
- [80] M. L. Good and W. D. Walker, Phys. Rev. **120** (1960) 1857.
- [81] T. CsddotOrgő, talk at “Low x 2017”, Bisceglie, June 13-17, 2017.
- [82] M. Froissart, *Phys. Rev.* **123** (1961) 1053;
A. Martin, “*Scattering Theory: Unitarity, Analyticity and Crossing.*” Lecture Notes in Physics, Springer-Verlag, Berlin-Heidelberg-New-York, 1969.
- [83] G. P. Lepage and S. J. Brodsky, Phys. Rev. Lett. **43** (1979) 545; Phys. Rev. Lett. **43** (1979) 1625.
- [84] I. Abt, A. M. Cooper-Sarkar, B. Foster, V. Myronenko, K. Wichmann and M. Wing, “*Does Nature Know about Perturbation Theory? A Study of HERA Deep Inelastic Scattering Data at Low Q^2 ,*” arXiv:1704.03187 [hep-ex].
- [85] A. H. Mueller, *Phys. Rev.* **D2** (1970) 2963.
- [86] Y. V. Kovchegov and K. Tuchin, Phys. Rev. **D65** (2002) 074026 [arXiv:hep-ph/0111362].
- [87] D. Kharzeev and E. Levin, Phys. Lett. B **523**, 79 (2001), [nucl-th/0108006].
- [88] K. Aamodt *et al.* [ALICE Collaboration], Eur. Phys. J. C **68** (2010) 89 [arXiv:1004.3034 [hep-ex]]; ALICE Collaboration, Eur. Phys. J. C **65** (2010) 111 [arXiv:0911.5430 [hep-ex]].
- [89] S. Chatrchyan *et al.* [CMS and TOTEM Collaborations], Eur. Phys. J. C **74** (2014) 10, 3053 [arXiv:1405.0722 [hep-ex]]; V. Khachatryan *et al.* [CMS Collaboration], Phys. Rev. Lett. **105**, 022002 (2010); [arXiv:1005.3299 [hep-ex]]. V. Khachatryan *et al.* [CMS Collaboration], JHEP **1002** (2010) 041 [arXiv:1002.0621 [hep-ex]].
- [90] ATLAS Collaboration, Phys. Lett. B **688** (2010) 21, arXiv:1003.3124 [hep-ex].
- [91] C. Amsler *et al.* (Particle Data Group), *Phys. Lett.* **B667** (2008) 1.